NJC

PAPER

View Article Online
View Journal | View Issue

Cite this: *New J. Chem.*, 2015, 39, 2669

Cage-like pores of a metal–organic framework for separations and encapsulation of Pd nanoparticles for efficient catalysis†

Yu Zhu,‡ Yan-Mei Wang,‡ Pan Liu, Yun-Long Wu, Wei Wei, Chang-Kun Xia and Ji-Min Xie*

Received (in Victoria, Australia) 8th November 2014,
Accepted 6th January 2015

DOI: 10.1039/c4nj01985g

www.rsc.org/njc

A porous metal–organic framework, $\{[Zn(BDC)_{1/2}(trz)]\cdot DMAC\}_n$ (Zn-BDC), was synthesized hydrothermally with the decomposition of 2,3-di(1,2,4-triazole)quinoxaline ligand (H_2BDC = 1,4-benzenedicarboxylic acid; Htrz = 1,2,4-1*H*-triazole). Structural analysis indicates the porosity of Zn-BDC with distorted oblong cages. Gas adsorption studies of N_2 and Ar on activated Zn-BDC reveal the BET surface areas of 587.3 and 519.5 $m^2\ g^{-1}$, respectively. Considering the certain size of the cages, Zn-BDC can separate organic compounds with different sizes through a MOF-column chromatographic method and deliver 5-fluorouracil, which can act as an anticancer drug. Zn-BDC has also been employed as a support for Pd nanoparticles. The results of catalytic hydrogenation of 4-nitrophenol demonstrate that the catalytic activity of Pd@Zn-BDC is superior enough compared to most Pd catalysts reported.

Introduction

Metal–organic frameworks (MOFs) or porous coordination polymers (PCPs) with adjustable permanent porosity and specific surface areas have been increasingly accelerated and sustained with extensive studies on some potential applications such as gas adsorption and separation,[1] chemical sensor and[2] heterogeneous catalysis.[3] In recent years, the surface area values of MOFs can be extended to about 10 000 $m^2\ g^{-1}$, which are better than traditional porous materials such as zeolites and carbons through ligands extension.[4] However, MOFs with larger pores often tend to collapse framework after the removal of guest molecules and cause interpenetration and self-interpenetration, decreasing the size of pores or channels.[5] Despite extensive success with MOFs possessing high surface area, it has presented tremendous opportunities to control the functionality in the framework and build new materials with unparalleled surface areas.[6] In some cases of MOFs, more than one type of ligand is applied to build a framework to expand the structural diversity, as well as to enhance physical properties. Designing the pore with specific sizes and shapes, the MOFs will be used for the separation of different organic molecules.

Recently, metal nanoparticles (MNPs) have been widely explored in the search for enhanced catalytic activities due to the active catalytic centers on the surface of MNPs.[7] However, pure MNPs with high surface energies and large surface areas are thermodynamically unstable and often accompanied by a decrease in catalytic activities because of the surface contamination nanoparticle aggregation.[8] In view of this, immobilizing the pure MNPs in the pores of MOFs as support has been proved to be an effective approach for the generation of free metal active sites reducing or even eliminating particle aggregation by controlling particle nucleation.[9] In the past, MOFs with high surface areas have been embedded with catalytically noble MNPs (Pd, Au, Ru, Cu and Pt) by employing various preparation methods, leading to green heterogeneous catalysts for higher catalytic activities.[10] MNPs larger than the cavities and particles can be often localized on the outer surface of the MOF crystallite, while smaller MNPs are embedded inside the MOF cavities, which are difficult to achieve. Moreover, facile and efficient approaches to embed MNPs onto MOFs with high stabilities and activities are still being explored and remain challenging due to the weak intermolecular interactions between metal–salt precursors and supports during the deposition.

Herein, 1,4-benzenedicarboxylic acid and 2,3-di(1,2,4-triazole)-quinoxaline were selected to construct a new MOF called Zn-BDC. However, 2,3-di(1,2,4-triazole)quinoxaline was decomposed under hydrothermal conditions. The structure consisted of BDC^{2-} anions and trz^{+} cations. Zn-BDC has cage-like pores, which can be used for the further immobilization of MNPs. Gas adsorptions demonstrate that the porous material has a BET

School of Chemistry and Chemical Engineering, Jiangsu University, Zhenjiang, 212013, P. R. China. E-mail: xiejm391@sohu.com

† Electronic supplementary information (ESI) available: PXRD patterns, TGA, FT-IR spectra, data of drug loading and delivery, tables of X-ray data, selected bond lengths and angle. CCDC 1022174. For ESI and crystallographic data in CIF or other electronic format see DOI: 10.1039/c4nj01985g

‡ Y. Zhu and Y. M. Wang contributed equally.

surface area of nearly 600 m^2 g^{-1}. Using a MOF-column chromatographic method, Zn-BDC can also separate organic compounds with different molecular sizes. Moreover, 5-fluorouracil (5-FU) can be loaded in the cages of Zn-BDC with the amount of 0.42 g g^{-1} and released in the body-like solution. After embedding the Pd NPs on Zn-BDC, the nano-material shows good dispersibility and superior catalytic activity for the hydrogenation of 4-nitrophenol.

Results and discussion

In order to understand the decomposition process of the ligand during the self-assembly of Zn-BDC, the organic compounds after solvothermal reaction were measured by GC analyses. Ethyl acetate was used to extract the organic phase of the solution after the reaction. GC analyses showed that most of the compound in ethyl acetate is 2,3-dichloroquinoxaline, which was derived from 2,3-di(1,2,4-triazole)quinoxaline (Fig. S2, ESI†). Thus, we can reasonably state the mechanism of the self-assembly process of Zn-BDC (Fig. 1): first, 2,3-di(1,2,4-triazole)quinoxaline was decomposed into two intermediates (trz^+ anion and quinoxaline cation). Deprotonation of trz^+ anion made it easier to be coordinated to the Zn ions and form the Zn-BDC crystals. On the other hand, the quinoxaline cation was finally transformed into 2,3-dichloroquinoxaline through the combination with Cl^- anions. To explore the role of the decomposition of 2,3-di(1,2,4-triazole)quinoxaline, we carried out two parallel experiments. Using H_2BDC/1,2,4-1*H*-triazole or H_2BDC/1,2,4-1*H*-triazole/2,3-dichloroquinoxaline with the same reaction condition, respectively, no crystals of Zn-BDC can be obtained (Fig. S3, ESI†). Thus, we can conclude that the decomposition plays an important role in the construction of Zn-BDC.

Single-crystal X-ray diffraction analysis reveals that Zn-BDC is constructed of dimetallic Zn clusters as secondary building units (SBUs) (Fig. 2), in which each Zn atom is five-coordinated with two O atoms from carboxylates and three N atoms from trz^+ cations. The bond length of Zn–O is 1.961(4) Å, while those of Zn–N are from 2.010(4) to 2.034(4) Å, which are similar to these bond lengths reported with similar structures.[11] Each SBU is connected *via* BDC^{2-} and trz^+ cations to form a fascinating three-dimensional open framework consisting of distorted bicapped square antiprism-shaped cages (Fig. 3) with windows of *ca.* 10.9 × 6.9 $Å^2$ from *b* axis (Fig. 4). A PLATON calculation

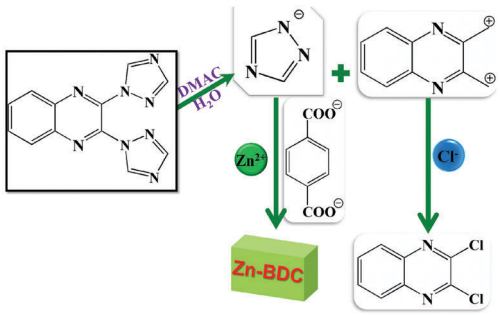

Fig. 1 The possible role of the decomposition of 2,3-di(1,2,4-triazole) quinoxaline in the construction of Zn-BDC.

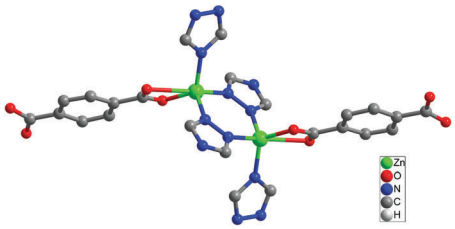

Fig. 2 Coordination environment of dimetallic Zn cluster in Zn-BDC.

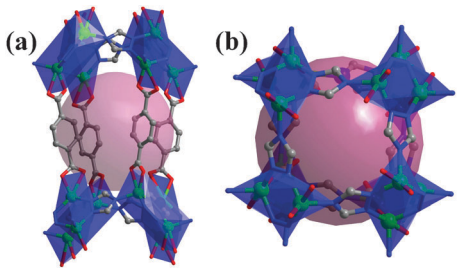

Fig. 3 (a) Distorted bicapped square antiprism-shaped cages viewed from *b* axis; (b) the cages viewed from *c* axis.

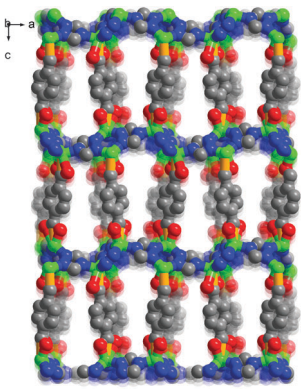

Fig. 4 The three-dimensional open framework with windows of *ca.* 10.9 × 6.9 $Å^2$ from *b* axis.

suggests a solvent-accessible volume of 2466.5 $Å^3$ (approximately 49.8% of the unit-cell volume) excluding the guest molecules. Park has ever reported a similar MOF of about 44.3% empty volume with the same ligands by a different procedure.[11] In addition to the difference of solvent-accessible volume, both the carboxylates groups in Zn-BDC are coordinated to the Zn ions with chelating mode, while only one carboxylates group is chelated to Zn ions. As a result, more stable and porous MOF was obtained finally during the special reaction process.

Based on the substantive weight loss from the TGA analysis (Fig. S5, ESI†) and the element analysis, there should be DMAC molecules inside the cages of Zn-BDC. The phase purity and the stability after the activation of Zn-BDC are confirmed by PXRD (Fig. S4, ESI†). For gas adsorption properties, activated Zn-BDC was selected to study the permanent porosities. As shown in Fig. 5, N_2 and Ar adsorption isotherms of Zn-BDC both reveal typical type-I behaviour, which is coincidental with the microporous structures.

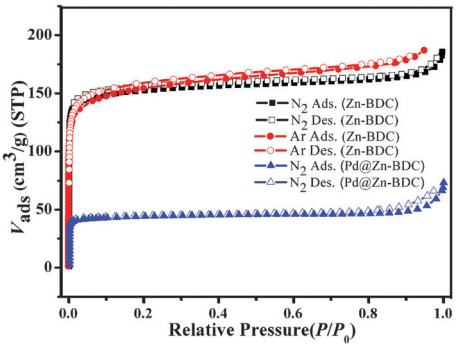

Fig. 5 N_2 (square points) and Ar (round points) adsorption isotherms for Zn-BDC and N_2 adsorption isotherm of Pd@Zn-BDC (triangle points).

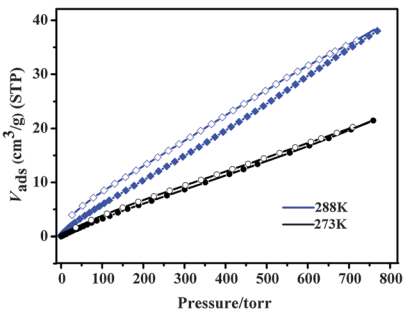

Fig. 6 CO_2 adsorption isotherms of Zn-BDC at 273 K and 288 K.

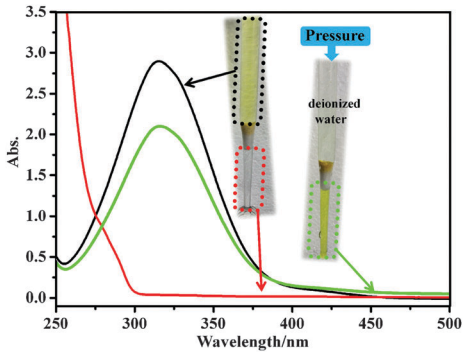

Fig. 7 Permeability of 4-NP in Zn-BDC based column with or without additional pressure, respectively.

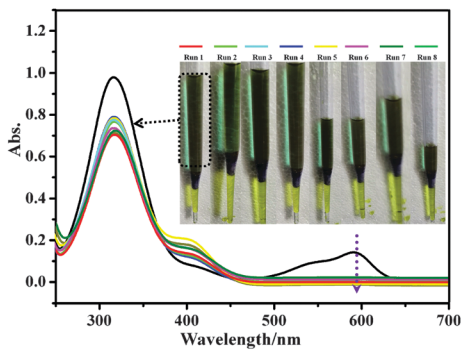

Fig. 8 Separation of CV–4-NP mixture with a Zn-BDC based column.

The uptakes of N_2 and Ar dramatically increase after pressurized and reach 185.5 cm^3 g^{-1} (STP) and 187.9 cm^3 g^{-1} (STP), respectively. N_2 adsorption indicates a surface area of 587.3 m^2 g^{-1} using the standard Brunauer–Emmett–Teller (BET) model. In addition, the surface area is calculated to be 519.5 m^2 g^{-1}, according to Ar adsorption. Using the Horvath–Kawazoe (HK) method,[12] the pore sizes of Zn-BDC distribution are 7.2 Å and 8.0 Å from N_2 and Ar adsorption isotherms, respectively, corresponding to the diameters of cages. Adsorption measurements of CO_2 were carried out up to about 800 torr. The CO_2 uptake of Zn-BDC is also very low, 38.6 cm^3 g^{-1} and 21.6 cm^3 g^{-1} at 273 K and 288 K, respectively (Fig. 6). In the structure, three N sites of triazole are all coordinated to the Zn^{2+} ions such that there are no functional groups to capture the CO_2 molecules, which cause the relatively low CO_2 uptakes.

Based on the size-exclusion effect, activated Zn-BDC powder has been employed as column-chromatographic filler for separating organic molecules with different sizes. Considering the pore size, 4-NP with yellow colour, which is easy to be distinguished was selected as a small template molecule. First, 4-NP solution was added to the column. After a few minutes, no 4-NP can transport through the column without pressure indicating the incorporated 4-NP inside the cages of Zn-BDC. After adding deionized water to the column with pressure using an aurilave, 4-NP was successfully passed through the column attributing to the smaller size of 4-NP than the channels of Zn-BDC (Fig. 7). Crystal violet (CV) with larger size was used as the unfavourable molecules. Generally, organic molecules with smaller size can pass through the pores of the MOFs, whereas larger molecules were excluded. To verify this, we used activated Zn-BDC to separate the mixture of CV–4-NP [m(dye) : m(4-NP) = 1 : 3] through a modified chromatographic column method.[13] Using this separation technique with additional pressure, CV–4-NP mixture can be easily and quickly separated by Zn-BDC, and it can be carried out for at least eight runs without obviously degenerative separating ability (Fig. 8). The principle of the separation can be explained as follows: the molecules of 4-NP can easily pass through the open framework of Zn-BDC with additional pressure, while CV molecules are too large and they can just stay outside the channels. To our knowledge, this is a rare example of a MOF-column chromatographic separation of organic compounds with different sizes, let alone the great efficiency of the separation.

Capacity of drug delivery was also evaluated using anticancer 5-FU, which is small enough to pass through the channels in view of the open framework. Adsorption of 5-FU was carried out by activated Zn-BDC with stirring in 5-FU containing methanol solution. Fluorescence spectroscopy has been used to determine the storage capacity of Zn-BDC; 21.05 mg of 5-FU can be absorbed by 50 mg of activated Zn-BDC (Fig. S8 and S9, ESI†). As a result, complete 5-FU loading was 0.42 g g^{-1} in Zn-BDC. A drug-release experiment was performed with Zn-BDC loaded with 5-FU. Seven milligrams of drug-loaded Zn-BDC was added to 3 mL of phosphate buffered saline (PBS) buffer solution (pH $\approx$ 7.4) at room temperature and measured by fluorescence spectrophotometer. The release process was observed with the "burst effect" (Fig. 9).

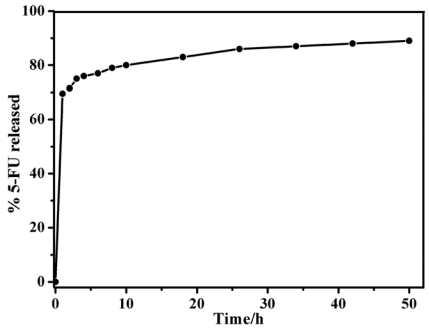

Fig. 9 The release process of 5-FU from the drug-loaded Zn-BDC (% 5-FU *vs.* time).

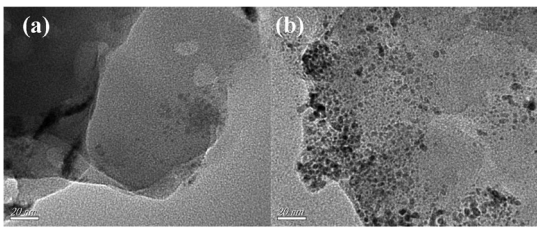

Fig. 10 (a) HRTEM image of Zn-BDC; (b) HRTEM image of Pd@Zn-BDC.

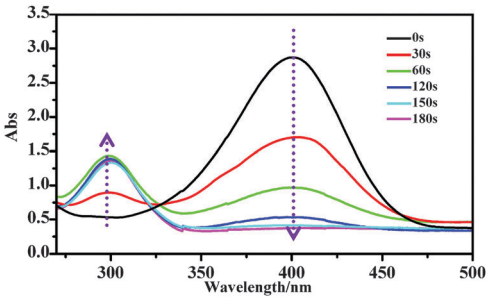

Fig. 11 UV-vis spectra of 4-NP reduction.

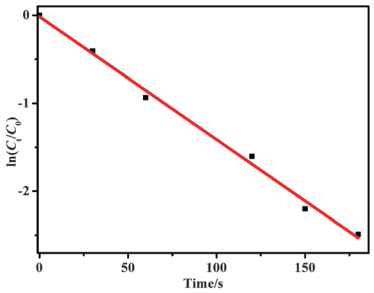

Fig. 12 Effect of Pd@Zn-BDC on the reduction rate of 4-NP.

In the first hour, 70.4% of the loaded drug was released. Then, the release of 5-FU became slower, and 89.5% was released in the later 49 h. The initial burst release of 5-FU may come from the drug molecules with weak intermolecular interactions in the open channel. After that, slow release of 5-FU may be due to drug molecules that are close to the channel walls, which are more difficult to release. The 5-FU molecules against the channel walls are mainly involved in host–guest interactions such as hydrogen bonds and π–π interactions between 5-FU and the organic part of the skeleton.[14]

MNPs have been widely explored on the extensive catalytic properties because of the catalytic sites on the surface. Herein, porous Zn-BDC is employed as a support for Pd embedded catalyst. PXRD patterns of Pd@Zn-BDC did not show apparent transformation of crystallinity (Fig. S6, ESI†). Two theta degrees of Pd NPs at about 40° and 46° can be observed clearly due to the higher Pd loading.[15] High-resolution TEM (HRTEM) images of Zn-BDC and Pd@Zn-BDC gave evidence for embedded Pd NPs with size distributions of 4–6 nm (Fig. 10). The Pd NPs are well dispersed on the surface of Zn-BDC and no apparent aggregation can be seen. N_2 adsorption isotherm of Pd@Zn-BDC shows the BET surface area of 175.1 $m^2\ g^{-1}$ with the pore size of 5.9 Å, which is smaller than that of Zn-BDC. To further confirm the catalytic activities of Pd NPs after being embedded onto Zn-BDC, we employed the liquid-phase reduction of 4-nitrophenol (4-NP) to 4-aminophenol (4-AP) by $NaBH_4$, which is directly catalyzed on the surface of the Pd NPs dispersed in solutions.[16] This model reaction has been widely employed to evaluate the catalytic activities of MNPs, and the reaction can be measured using a UV-vis spectroscope from which a full kinetics study can be completed. As we know, 4-NP cannot be reduced by aqueous $NaBH_4$ in the absence of metal NPs.[17] However, after adding Pd@Zn-BDC catalyst, the reduction reaction can be observed, and the absorption peak at 400 nm of 4-NP decreased quickly along with an increase of the 300 nm peak of 4-AP concomitantly (Fig. 11). The complete reduction of 4-NP was achieved within 180 s over the Pd@Zn-BDC catalyst. The overall kinetic analysis of the 4-NP reduction reaction is presented as $\ln(C_t/C_0) = -kt$, where k is the kinetic rate constant and C_0 and C_t are the initial and apparent concentrations of 4-NP, respectively.[18] The $\ln(C_t/C_0)$ is plotted as a function of time, in which the slope of the best fit line represents the $-k$ value of the reaction. A linear relationship between $\ln(C_t/C_0)$ and time (t) was observed indicating a pseudo-first order reaction with the $k = 0.014\ s^{-1}$ (Fig. 12). As a comparison, Zn-BDC was utilized as catalysts for the catalytic reaction. However, no obvious catalytic activity was observed. As a result, the catalyst with embedded Pd NPs has great effects on the catalytic properties. The probable mechanism of high activity may be explained as follows: first, a large amount of 4-NP with small size can be absorbed around the channel of Pd@Zn-BDC due to the porosity. Then, the electrons from BH_4^- transfer to Pd NPs, and subsequently the 4-NP absorbed on the catalyst surface takes electrons and transforms to 4-AP.[19] Then, 4-AP gets through the channels and made the sustainability and efficiency of the catalytic reaction by the Pd NPs with small particle size, which makes the comparable conversion.[18,20] In addition, the catalyst did not show apparent loss of the activities after five cycles, indicating the stability of the catalyst (Fig. S12, ESI†).

Conclusions

In conclusion, a porous metal–organic framework called Zn-BDC was synthesized with distorted oblong cages. Zn-BDC can be applied for MOF-column chromatographic separation of organic

compounds with different sizes and drug delivery of 5-fluorouracil. After embedding Pd NPs, Pd@Zn-BDC shows high catalytic reduction of 4-nitrophenol.

Experimental

Materials and physical measurements

The synthesis of 2,3-di(1,2,4-triazole)quinoxaline has been reported in our previous work.[21] Other materials employed were purchased from commercial sources and used as received without further purification. Elemental analyses for C, H and N were determined with a Perkin-Elmer 240, and the Pd contents were determined by inductively coupled plasma-optical emission spectrometry (ICP-OES) on a Varian Vista MPX instrument. Fourier transform infrared (FTIR) spectra were measured as KBr pellets on a Nicolet FT-170SX spectrometer in the range of 400–4000 cm^{-1}. Thermogravimetric analysis (TGA) experiments were carried out on an integrated thermal STA 449C analyzer heated from room temperature to 800 °C under N_2 atmosphere. Powder X-ray diffraction (PXRD) patterns were collected on a Rigaku D/max2500VB3+/PC diffractometer equipped with Cu-Kα radiation (λ = 1.5406 Å). The morphology of Pd@Zn-BDC was investigated by High Resolution Transmission Electron Microscope JEM-2100 (HRTEM). The UV-vis spectra were measured on UV-2450 spectrophotometer. The UV-vis spectra were measured on UV-2450 spectrophotometer. Gas chromatography analyses were carried out on Agilent 7890A.

Synthesis of $\{[Zn(BDC)_{1/2}(trz)]\cdot DMAC\}_n$ (Zn-BDC). A mixture of the H_2BDC (0.017 g, 0.1 mmol), 2,3-di(1,2,4-triazole)quinoxaline (0.026 g, 0.1 mmol) and $ZnCl_2$ (0.027 g, 0.2 mmol) in H_2O and DMAC mixture (1 : 1, 3 mL) was placed in a Parr Teflon-lined stainless steel vessel and heated to 90 °C for 3 days. The reaction was cooled to room temperature slowly, and then yellow crystals were obtained. After filtration, the crystals were washed with H_2O and dried in air. Anal. Calcd for $C_{10}H_{13}N_4O_3Zn$ (M_r = 302.61): C, 39.69; H, 4.33; N, 18.51%. Found: C, 39.55; H, 4.48; N, 18.48%. IR (cm^{-1}, KBr pellet): 3612(w), 3527(w), 3139(w), 3102(m), 2936(w), 1624(s), 1592(s), 1525(s), 1505(m), 1398(s), 1368(s), 1299(m), 1270(w), 1218(m), 1170(m), 1144(w), 1091(s), 1039(m), 1007(s), 921(w), 841(s), 752(s), 669(s), 589(w), 572(w), 475(w).

Synthesis of Pd@Zn-BDC. $Pd(OAc)_2$ (28 mg, 0.11 mmol) was dissolved in 3 mL acetone, and activated Zn-BDC crystals (22 mg, 0.1 mmol) were placed into the Pd-based solution for 24 hours quietly at room temperature. The solid was obtained after centrifugation and washed with acetone (3 × 10 mL) and then slowly dried under vacuum at 50 °C for 8 h to obtain brown Pd(II)@Zn-BDC powder. Pd@Zn-BDC was then synthesized with the reduction by $NaBH_4$ (19 mg, 0.5 mmol) at 0 °C for 3 h. The Pd loading on the sample was 1.7 wt% based on ICP analysis.

X-ray crystallography

The X-ray intensity data for the compounds were collected on a Rigaku Saturn 724+ CCD diffractometer with graphite monochromatized Mo Kα radiation (λ = 0.71073 Å). The crystal structure was solved by direct methods using difference Fourier synthesis with SHELXTS[22] and refined by full-matrix least-squares method using the SHELXL-97 program.[23] The non-hydrogen atoms were refined with anisotropic displacement parameters. The solvent molecules were highly disordered and impossible to find in the Fourier maps and fixed in the ideal position.[24] To resolve this issue, the contribution of solvent electron density was removed by SQUEEZE routine in PLATON.[25] The molecules removed were determined with recovered number of electrons in the void by SQUEEZE, as well as elemental analysis and TGA data. Crystal data and details of the structure determination for the compound are listed in Table S1 (ESI†).

Gas adsorption measurements

Prior to gas adsorption experiments, the samples were soaked in methanol to exchange DMAC solvents, which was then followed by evacuation under a dynamic vacuum at 120 °C for the 8 hours. All the gas adsorption isotherms were measured using a Micromeritics ASAP 2020 analyzer employing a standard volumetric technique up to saturated pressure. The N_2 and Ar adsorption isotherms were monitored at 77 K and 87 K, respectively, while CO_2 adsorption isotherms were obtained at 273 K and 288 K. The adsorption data were refitted to the Brunauer–Emmett–Teller (BET) equation to determine the surface areas.

Separation with Zn-BDC column

Using methanol to exchange DMAC solvents and evacuating under a dynamic vacuum at 120 °C for the 8 hours, activated Zn-BDC was finally obtained. Then, the ground powder was added to a clean dropper and compressed with water. The separation of CV–4-NP mixture should be carried out with pressure additionally which was provided by an aurilave.

Drug loading and delivery

Adsorption of anticancer 5-fluorouracil was carried out by impregnating activated Zn-BDC (50 mg) under stirring in 5-FU (100 mg) containing methanol solutions for 2 days. Fluorescence spectroscopy at a detection wavelength of about 410 nm has been used to determine the storage capacity by drawing a standard curve. Then, 7 mg drug-loaded Zn-BDC was added to 3 mL of a PBS solution at room temperature to test the release ability. At time intervals, the solution was sampled for determining the drug concentration.

Catalytic reaction of reduction of 4-nitrophenol (4-NP) to 4-aminophenol (4-AP)

Typically, 180 mg of $NaBH_4$ was dissolved in 10 mL deionized water and then mixed with 20 mL deionized water of 7 mg 4-NP. The mixture was stirred for 2 min, and 5 mg of catalyst was then added. After introducing the catalyst, the bright yellow solution turned clear gradually. UV-vis spectra of the solution were measured during the course of the reaction.

Acknowledgements

This work was partly supported by National Natural Science Foundation of China (21171075/B010303, 21103073/B030201

and 21306067/B060903), Science & Technology Supporting Program of Jiangsu Province of China (BE2013090) and Innovation project for graduate student research of Jiangsu Province (No. cxzz13_0679).

Notes and references

1 J. R. Li, J. Yu, W. Lu, J. Sculley, P. B. Balbuena and H. C. Zhou, *Nat. Commun.*, 2013, **4**, 1538; Y. Zhu, Y. M. Wang, S. Y. Zhao, P. Liu, C. Wei, Y. L. Wu, C. K. Xia and J. M. Xie, *Inorg. Chem.*, 2014, **53**, 7692–7699; J. R. Li, J. Sculley and H. C. Zhou, *Chem. Rev.*, 2012, **112**, 869–932; A. M. Fracaroli, H. Furukawa, M. Suzuki, M. Dodd, S. Okajima, F. Gándara, J. A. Reimer and O. M. Yaghi, *J. Am. Chem. Soc.*, 2014, **136**, 8863–8866.

2 H. L. Jiang, D. Feng, K. Wang, Z. Y. Gu, Z. Wei, Y. P. Chen and H. C. Zhou, *J. Am. Chem. Soc.*, 2013, **135**, 13934–13938; Y. Zhu, Y. M. Wang, J. Xu, P. Liu, H. D. Weththasinha, Y. L. Wu, X. Q. Lu and J. M. Xie, *J. Solid State Chem.*, 2014, **219**, 259–264; Y. J. Cui, Y. F. Yue, G. D. Qian and B. L. Chen, *Chem. Rev.*, 2012, **112**, 1126–1162; P. Y. Wu, J. Wang, Y. M. Li, C. He, Z. Xie and C. Y. Duan, *Adv. Funct. Mater.*, 2011, **21**, 2788–2794.

3 W. Y. Gao, Y. Chen, Y. H. Niu, K. Williams, L. Cash, P. J. Perez, L. Wojtas, J. F. Cai, Y. S. Chen and S. Q. Ma, *Angew. Chem., Int. Ed.*, 2014, **53**, 2615–2619; R. Haldar, S. K. Reddy, V. M. Suresh, S. Mohapatra, S. Balasubramanian and T. K. Maji, *Chem. – Eur. J.*, 2014, **20**, 4347–4356; Y. M. Wang, Y. Zhu, J. Xu, C. Wei, P. Liu, Y. L. Wu and J. M. Xie, *Polyhedron*, 2014, **81**, 32–38.

4 H. Furukawa, K. E. Cordova, M. O'Keeffe and O. M. Yaghi, *Science*, 2013, **341**, 1230444.

5 D. Han, F. L. Jiang, M. Y. Wu, L. Chen, Q. H. Chen and M. C. Hong, *Chem. Commun.*, 2011, **47**, 9861–9863.

6 T. Park, A. J. Hickman, K. Koh, S. Martin, A. G. Wong-Foy, M. S. Sanford and A. J. Matzger, *J. Am. Chem. Soc.*, 2011, **133**, 20138–20141.

7 A. Aijaz and Q. Xu, *J. Phys. Chem. Lett.*, 2014, **8**, 1400–1411; Y. G. Sun and Y. N. Xia, *Science*, 2002, **298**, 2176–2179; Y. Y. Liu, W. N. Zhang, S. Z. Li, C. L. Cui, J. Wu, H. Y. Chen and F. W. Huo, *Chem. Mater.*, 2014, **26**, 1119–1125; V. P. Taori, R. Bandari and M. R. Buchmeiser, *Chem. – Eur. J.*, 2014, **20**, 3292–3296; R. Bandari, T. Hoche, A. Prager, K. Dirnberger and M. R. Buchmeiser, *Chem. – Eur. J.*, 2010, **16**, 4650–4658; R. Bandari and M. R. Buchmeiser, *Catal. Sci. Technol.*, 2012, **2**, 220–226.

8 J. P. Ge, Q. Zhang, T. R. Zhang and Y. D. Yin, *Angew. Chem., Int. Ed.*, 2008, **47**, 8924–8928.

9 J. Hermannsdorfer, M. Friedrich, N. Miyajima, R. Q. Albuquerque, S. Kummel and R. Kempe, *Angew. Chem., Int. Ed.*, 2012, **51**, 11473–11477.

10 X. J. Gu, Z. H. Lu, H. L. Jiang, T. Akita and Q. Xu, *J. Am. Chem. Soc.*, 2011, **133**, 11822–11825; Y. B. Huang, Z. J. Lin and R. Cao, *Chem. – Eur. J.*, 2011, **17**, 12706–12712; D. Esken, S. Turner, O. I. Lebedev, G. V. Tendeloo and R. A. Fischer, *Chem. Mater.*, 2010, **22**, 6393–6401; Y. Y. Pan, B. Z. Yuan, Y. W. Li and D. H. He, *Chem. Commun.*, 2010, **46**, 2280–2282; F. Ke, J. F. Zhu, L. G. Qiu and X. Jiang, *Chem. Commun.*, 2013, **49**, 1267–1269; Q. L. Zhu and Q. Xu, *Chem. Soc. Rev.*, 2014, **43**, 5468–5512.

11 H. Park, D. M. Moureau and J. B. Parise, *Chem. Mater.*, 2006, **18**, 525–531.

12 M. Jaroniec, J. Choma and M. Kruk, *Colloids Surf., A*, 2003, **214**, 263–269.

13 Y. Q. Lan, H. L. Jiang, S. L. Li and Q. Xu, *Adv. Mater.*, 2011, **23**, 5015–5020.

14 D. Zhao, S. W. Tan, D. Q. Yuan, W. G. Lu, Y. H. Rezenom, H. L. Jiang, L. Q. Wang and H. C. Zhou, *Adv. Mater.*, 2011, **23**, 90–93; Y. Wang, J. Yang, Y. Y. Liu and J. F. Ma, *Chem. – Eur. J.*, 2013, **19**, 14591–14599.

15 J. Hermannsdorfer and R. Kempe, *Chem. – Eur. J.*, 2011, **17**, 8071–8077.

16 R. Bhandari and M. R. Knecht, *ACS Catal.*, 2011, **1**, 89–98.

17 Z. F. Jiang, J. M. Xie, D. L. Jiang, J. J. Jing and H. R. Qin, *CrystEngComm*, 2012, **14**, 4601–4611.

18 C. Deraedt, L. Salmon, J. Ruiz and D. Astruc, *Adv. Synth. Catal.*, 2013, **355**, 2992–3001.

19 F. Ke, J. F. Zhu, L. G. Qiu and X. Jiang, *Chem. Commun.*, 2013, **49**, 1267–1269.

20 X. M. Gu, W. Qi, X. Z. Xu, Z. H. Sun, L. Y. Zhang, W. Liu, X. L. Pan and D. S. Su, *Nanoscale*, 2014, **6**, 6609–6616.

21 J. Chen, Y. Zhu, Y. L. Wu, C. K. Xia and J. M. Xie, *Chem. Reag.*, 2013, **35**, 773–776.

22 G. M. Sheldrick, *SHELXS-97, Program for Automatic Solution of Crystal Structures*, University of Göttingen, Göttingen, Germany, 1997.

23 G. M. Sheldrick, *SHELXL-97, Program for Crystal Structure Refinement*, University of Göttingen, Göttingen, Germany, 1997.

24 L. Qin, J. S. Hu, Y. Z. Li and H. G. Zheng, *Cryst. Growth Des.*, 2011, **11**, 3115–3121.

25 L. F. Wang, L. C. Kang, W. W. Zhang, F. M. Wang, X. M. Ren and Q. J. Meng, *Dalton Trans.*, 2011, **40**, 9490–9497.

